



## Columnar Lithium Metal Anodes

Xue-Qiang Zhang<sup>+</sup>, Xiang Chen<sup>+</sup>, Rui Xu<sup>+</sup>, Xin-Bing Cheng<sup>+</sup>, Hong-Jie Peng, Rui Zhang, Jia-Qi Huang, and Qiang Zhang\*

**Abstract:** The rechargeable lithium metal anode is of utmost importance for high-energy-density batteries. Regulating the deposition/dissolution characteristics of Li metal is critical in both fundamental researches and practical applications. In contrast to gray Li deposits featured with dendritic and mossy morphologies, columnar and uniform Li is herein plated on lithium-fluoride (LiF)-protected copper (Cu) current collectors. The electrochemical properties strongly depended on the microscale morphologies of deposited Li, which were further embodied as macroscale colors. The as-obtained ultrathin and columnar Li anodes contributed to stable cycling in working batteries with a dendrite-free feature. This work deepens the fundamental understanding of the role of LiF in the nucleation/growth of Li and provides emerging approaches to stabilize rechargeable Li metal anodes.

High-energy-density, low-cost, and safely rechargeable batteries are intensively requested with the rapid development of portable electronics, electric vehicles, and smart electric grids.<sup>[1]</sup> Li metal is considered a very promising anode material for battery applications due to its high theoretical specific capacity (3860 mAhg<sup>-1</sup>) and extremely low reduction potential (−3.04 V vs. standard hydrogen electrode).<sup>[2]</sup> However, uncontrollable Li deposition/dissolution during repeated plating/stripping processes, usually embodied as dendritic and mossy Li featured with a gray color, induces a series of thorny issues, such as low Coulombic efficiency (CE), short circuit, and even fire/explosion of batteries.<sup>[3,4]</sup>

In general, the solid electrolyte interphase (SEI) between the Li metal and the organic electrolyte is structurally fragile and compositionally heterogeneous (Figure 1 a). The fragility and heterogeneity render the extremely sporadic nucleation sites for Li deposition.<sup>[5]</sup> It is kinetically preferred for Li ions to be plated on these existing nucleation sites, giving rise to

large and sparsely distributed hemispherical Li bumps and finally a moss- and tuber-like morphology. Over the past decades, many efforts have been devoted to regulating the deposition/dissolution characteristics of Li metal, raising several effective methods to suppress the growth of Li dendrites, such as SEI regulation,<sup>[6]</sup> physical blocking barriers,<sup>[7]</sup> uniformization of the Li-ion flux,<sup>[8]</sup> and three-dimensional lithiophilic scaffolds.<sup>[9]</sup> Many of them indicate the important role of the initial state of SEI in directing the subsequent plating/stripping. If the initial nucleation/growth is well-regulated by a stable and homogenous SEI, the subsequent deposition/dissolution of Li metal will be steady and uniform.

Based on this consideration, the concept of depositing Li onto Cu current collectors with a LiF-rich initial surface is explored to guide the uniform deposition of Li metal. LiF is selected to regulate the formation of initial SEI due to its very high surface diffusivity for Li ions, which has been proved to render a feasibility to suppress dendritic Li growth in working batteries.<sup>[10]</sup> A columnar and uniform Li metal film is therefore obtained through the regulation of LiF (Figure 1 b). The noteworthy correlation between the microscale morphology, the electrochemical plating/stripping conditions, and the

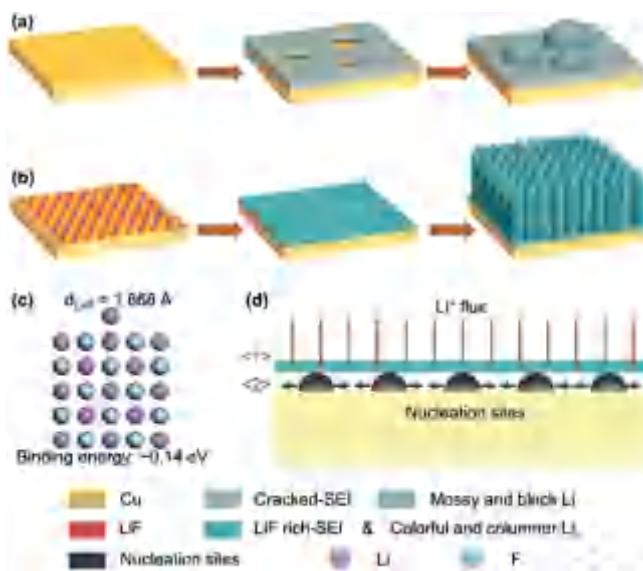


**Figure 1.** Schematics for the Li plating morphologies on different substrates: a) bare Cu with an unmodified and easily cracked SEI and b) modified Cu with a LiF-rich surface to render a columnar morphology of deposited Li. Theoretical modeling: c) binding energy of Li on LiF (100) surface and d) schematic showing the whole LiF-regulated Li deposition, (1) LiF-rich SEI contributes to even spatial distribution of Li ions, (2) uniform and dense nucleation sites are formed on Cu and grows horizontally from these nucleation sites.

[\*] X.-Q. Zhang,<sup>[†]</sup> X. Chen,<sup>[†]</sup> Dr. X.-B. Cheng,<sup>[†]</sup> H.-J. Peng, R. Zhang, Prof. Q. Zhang  
Beijing Key Laboratory of Green Chemical  
Reaction Engineering and Technology  
Department of Chemical Engineering, Tsinghua University  
Beijing 100084 (P. R. China)  
E-mail: zhang-qiang@mails.tsinghua.edu.cn

R. Xu,<sup>[†]</sup> Prof. J.-Q. Huang  
Advanced Research Institute for  
Multidisciplinary Science  
Beijing Institute of Technology  
Beijing 100081 (P. R. China)

[†] These authors contributed equally to this work.

Supporting information and the ORCID identification number(s) for the author(s) of this article can be found under:  
<https://doi.org/10.1002/anie.201707093>.

macroscale color of Li are unveiled. In addition, the as-obtained ultrathin and columnar Li metal anodes are demonstrated in various battery prototypes with extended cycling lives.

LiF particles were coated on routine planar Cu current collectors (denoted as LiF-rich Cu) by in situ hydrolysis of lithium hexafluorophosphate ( $\text{LiPF}_6$ ) when a piece of Cu foil was immersed into an aqueous  $\text{LiPF}_6$  solution. The hydrolyzing products of  $\text{LiPF}_6$  mainly include LiF and hydrogen fluoride.<sup>[11]</sup> The mild hydrolysis rendered the Cu foil with an amorphous LiF-rich surface and concurrently the pristine oxide layer on Cu was facilely removed, which will be indicated in the following contents. Through theoretical modeling based on first-principles calculations, Li atoms were found to be weakly adsorbed on the LiF (100) surface with a binding energy of  $-0.14$  eV (Figure 1 c), which is much smaller than  $-2.57$  eV on Cu (100).<sup>[12]</sup> In addition, the diffusion energy barrier of Li on LiF (100) surface is slightly higher than on Cu (100) but still sufficiently low to construct rapid Li-ion-diffusion paths within the SEI (see Figure S1 in the Supporting Information).<sup>[13]</sup> In combination with its uniform coating on a Cu foil, the LiF layer, with high Li-ion diffusivity, renders uniform and small interfacial resistance, further leading to even spatial distribution of Li ions, as well as an aligned column structure (Figure 1 d).<sup>[14]</sup> When these Li ions uniformly penetrate through the SEI, they are subsequently adsorbed to Cu owing to the substantially higher binding energy than to LiF and then reduced by electrons from the current collector to form dense nucleation sites. The facile nucleation is in good accordance with the lower nucleation overpotential on LiF-rich Cu than bare Cu (Figure S2a). Because of the low diffusion energy barrier, Li rapidly diffuses on Cu and thus grows horizontally from these nucleation sites. After contacting with each other, Li deposits then grow vertically under the spatial confinement and finally evolve into self-aligned columns. The adjacent nucleation sites are prevented from merging by the SEI that are coated on each column. Such a unique ordered aligned columnar structure of Li on LiF-rich Cu is evidenced as the origin of coloring of Li in the following content.

Performed in an electrolytic bath, the Li deposition on routine Cu and LiF-rich Cu exhibited totally different colors and morphologies (Figures 2 and S2). The color of deposited Li on bare Cu is gray (Figure 2a). During the Li plating, Li ions are preferentially attracted by existing nucleation sites, which are sparsely distributed due to the large spatial variations in interfacial resistance across the unmodified SEI. As a result, Li grew into separated hemispherical bumps (Figure 2a). A moss- and tuber-like morphology was therefore obtained once more Li metal was deposited.

In contrast, the deposited Li on the LiF-rich Cu foil possesses a color of brilliant blue and a self-aligned columnar morphology (Figure 2b). The diameter of the columnar Li is about 300 nm and within a narrow distribution (Figure S2b and c). The Li film is about 5- $\mu\text{m}$  thick, which is much thinner than that of a commercial Li foil (ca. 200  $\mu\text{m}$ ) and corresponds to a deposition capacity of 1.0  $\text{mAhcm}^{-2}$  (Figure 2c). More interestingly, the columnar Li presents different colors when observed at different light incident angles, resembling to the

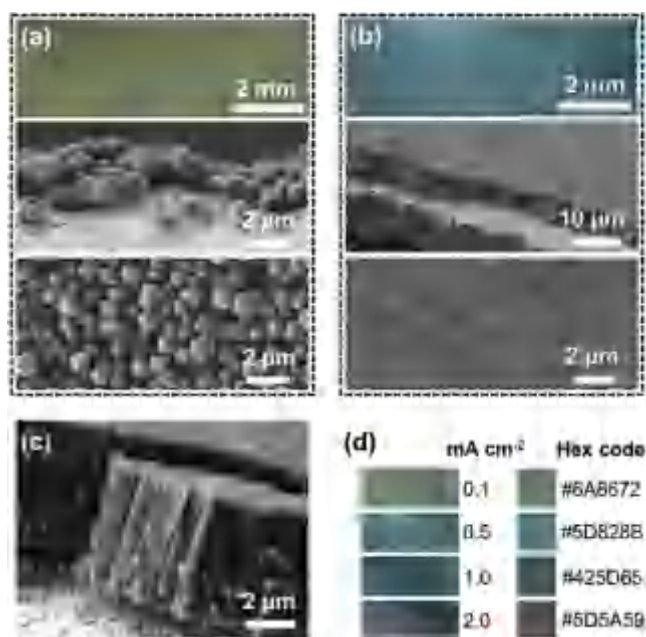


**Figure 2.** The morphology of Li (deposition capacity: 1.0  $\text{mAhcm}^{-2}$ ; current density: 0.5  $\text{mAcm}^{-2}$ ; carbonate electrolyte) on a) bare Cu and b) LiF-rich Cu, showing (upper) optical photos of deposited Li films in a light incident angle of  $45^\circ$ , (middle) cross-sectional, and (bottom) top-view scanning electron microscopy (SEM) images of Li deposits. c) High-magnification and cross-sectional SEM image of columnar Li growing on LiF-rich Cu. d) A series of optical photos of columnar Li deposited at different current densities of 0.1, 0.5, 1.0, and 2.0  $\text{mAcm}^{-2}$ , and the corresponding hex codes of their structural colors.

structural colors of *Morpho* butterfly (Figure S3).<sup>[15]</sup> Such dendrite-free blueish Li deposits was also described by Zhang and co-workers whereas a different electrolyte consisting of 1.0 M  $\text{LiPF}_6$  and 0.05 M cesium hexafluorophosphate in propylene carbonate was employed.<sup>[16]</sup> The formation of such a compact aligned Li columnar structure is preceded by a SEI layer formed on the surface of the Cu, which will be explained later.

To demonstrate the universality of columnar Li, the influence of current density was unraveled. When the current density decreased to 0.10  $\text{mAcm}^{-2}$ , the columnar morphology of Li deposits was maintained (Figure S4d and g) but displayed a color of cyan (Figure 2d). Increasing the current density to 1.0 and 2.0  $\text{mAcm}^{-2}$  hardly induced changes in the columnar morphology but the color turned into dark navy and violet, respectively (Figure S4b, e, and f, and S4c, f, and i). The structural color originates from the interactions between the visible light and ordered microstructures. Similarly, the coloring of Li films, which are argenteous and gray before and after cycling under routine conditions, is attributed to the ordered columnar microstructure. The colors of these columnar Li deposits transit from cyan to dark violet with the increase in plating current density, agreeing with the decrease in the light wavelength. Such a decrease is fully consistent with the reduced diameter of columnar Li (Figure S5). Such a consistent tendency of color change enables a preliminary but quite fast and direct method to evaluate the status of a cycled Li

metal anode by simply examining its color. However, the diameter uniformity was partially disturbed at a high current density (e.g.  $2.0 \text{ mA cm}^{-2}$ ), suggesting that large current density is unfavorable to uniform Li deposition.

The morphology evolution of columnar Li during the whole plating process was also recorded. Li deposited with a capacity of 0.25 and  $0.50 \text{ mAh cm}^{-2}$  at  $0.5 \text{ mA cm}^{-2}$  kept aligned and uniform (Figure S6). The thickness of Li film increased from 1.2 to  $2.4 \mu\text{m}$ , which was roughly proportional to the deposition capacity and thus confirmed the uniform and vertical growth of columns. After one cycle, Li deposited on bare Cu was still in gray color but the Li particles became much less compact and more uneven than before (Figure S7a and c). In contrast, the brilliant blue color, as well as the columnar microstructures, was preserved for the Li deposited on LiF-rich Cu, demonstrating a good reversibility of columnar Li during cycling (Figure S7b and d). In addition, Li roots are intentionally peeled off from a stainless steel substrate to visualize the uniform and dense nucleation sites beneath the LiF-rich protective film (Figure S8).

To reveal the origin of different Li deposition behaviors, the surfaces of two Cu substrates were further probed. The LiF-rich Cu substrate is brighter than bare Cu, suggesting a more even surface, which is further indicated by the SEM images showing the uniform coating of LiF nanoparticles (Figure 3a and b). The distinct surface chemistry of bare Cu and LiF-rich Cu was also detected by X-ray photoelectron

spectroscopy (XPS) (Figure 3c). In the Cu 2p spectra, there are mainly three sets of peak assigning to  $\text{Cu}^{2+}$  ( $934.8/954.8 \text{ eV}$  for  $\text{Cu}^{2+} 2p^{3/2}/2p^{1/2}$ ),  $\text{Cu}^0$  ( $932.7/952.7 \text{ eV}$  for  $\text{Cu} 2p^{3/2}/2p^{1/2}$ ), and satellite peaks of  $\text{Cu}^{2+}$  ( $941.1, 943.8$  and  $962.3 \text{ eV}$ ), respectively (Figure 3d and f). On bare Cu surface, the major species are suggested to be  $\text{Cu}^{2+}$  due to the native oxide layer. On LiF-rich Cu, however, the peaks of  $\text{Cu}^{2+}$  are not detected and the signals of  $\text{Cu}^0$  are obviously strengthened, suggesting the removal of surface oxide film and the exposure of Cu metal. Besides, bare Cu exhibits no signal of F; while there is a unimodal peak attributed to LiF in the F 1s spectrum of LiF-rich Cu (Figure 3c and e). The existence of F element is further indicated by energy dispersive spectroscopy (Figure S9). The emergence of LiF is the most evident difference between bare Cu and LiF-rich Cu, which is also what the growth of columnar Li metal originates from.

The SEI on deposited Li also plays a critical role in the Li plating process. The distribution of fluorine element is more uniform in SEI of Li film on LiF-rich Cu (Figure S10). The XPS spectra further indicates the increased content of LiF in the SEI of the Li film on the LiF-rich Cu (Figure S11). The significant peak of  $-\text{CF}_3$  ( $293.1 \text{ eV}$ ) in the C 1s spectrum of Li on LiF-rich Cu cannot be detected; while in the F 1s spectra, the ratios between LiF ( $684.7 \text{ eV}$ ) and  $-\text{CF}_3$  ( $688.6 \text{ eV}$ ) are inverse for the SEI of the Li films on bare Cu and LiF-rich Cu. All these results evidence that the SEI of Li on LiF-rich Cu is dominated by rich LiF as expected. The pristine LiF-rich layer derived from the hydrolysis of  $\text{LiPF}_6$  can be well-preserved, which persistently facilitates the uniform spatial distribution of Li ion transportation towards stable Li plating into columnar Li film.

Electrochemical tests in both carbonate and ether electrolytes were performed to evaluate the Li metal anode on LiF-rich Cu in a working coin cell. The Li deposition after one cycle was smooth and dense on LiF-rich Cu but dendritic on bare Cu in carbonate electrolyte (Figure S12). As the plating occurred in space-confined coin cells, the morphology was different from that deposited in the electrolytic bath.

Figure 4a exhibits the CE of Li|Cu coin cells based on a carbonate electrolyte with a capacity of  $1.0 \text{ mAh cm}^{-2}$  at  $0.5 \text{ mA cm}^{-2}$ . The CEs of cells with LiF-rich Cu and bare Cu are nearly the same (85%), which agree well with the previous reports.<sup>[3,17]</sup> In particular, the initial CE (94%) is much higher than that of bare Cu (85%), strongly demonstrating the critical role of initial LiF-rich surface. The CE of the bare-Cu cell decreases rapidly after only 70 cycles; however, the CE of the cell applying LiF-rich Cu maintains stable during 140 cycles. When the Li anode on LiF-rich Cu was tested in ether electrolyte with 2 wt % lithium nitrate as additive, the CE could be improved to 98.7% and maintained within 120 cycles (Figure 4b). In contrast, high CE of the bare-Cu cell can only be preserved within 45 cycles. The enhanced CE and lifespan were also significant when the current density was increased to  $1.0 \text{ mA cm}^{-2}$  (Figure S13). The polarization voltage of cells based on LiF-rich Cu maintains stable during cycling (Figure 4c). The resistance of the SEI formed on LiF-rich Cu is nearly half of that on bare Cu, confirming the role of LiF in decreasing the SEI resistance (Figure 4d). In addition, the cycling performance

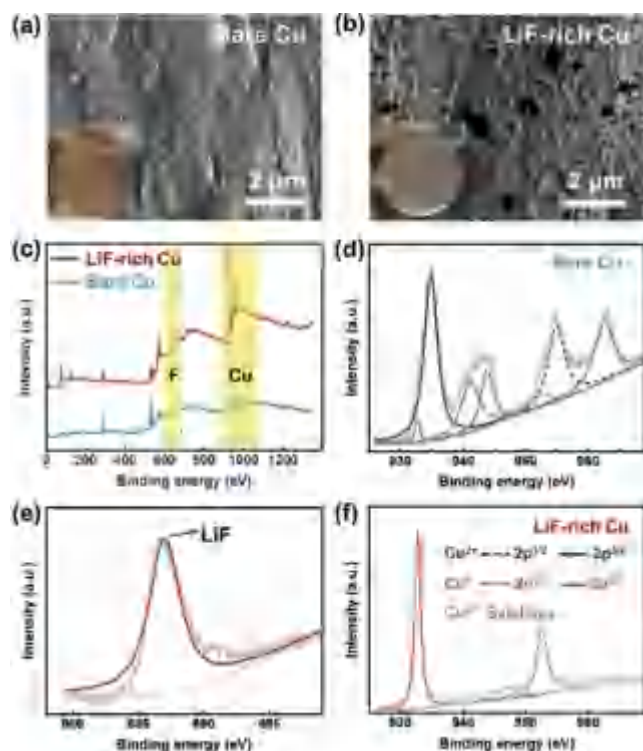


**Figure 3.** Morphology and composition of bare Cu and LiF-rich Cu substrates. SEM images and inset photos of a) bare Cu and b) LiF-rich Cu. c) The XPS spectra of bare Cu and LiF-rich Cu foil. Fine-scanning d) Cu 2p spectra of bare Cu, e) F 1s, and f) Cu 2p spectra of LiF-rich Cu.

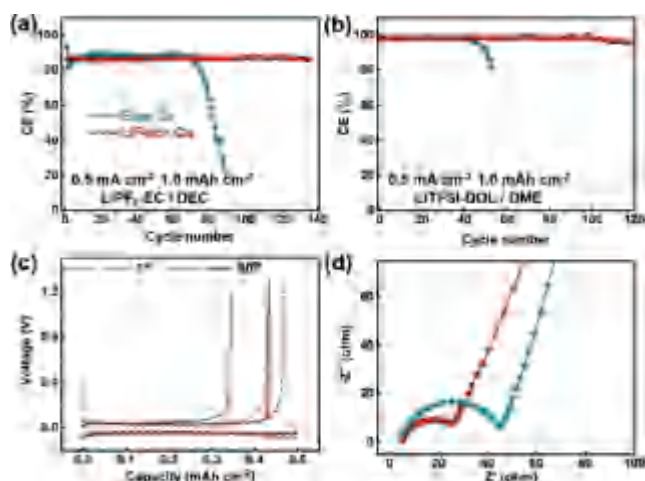


**Figure 4.** Electrochemical performance of Li | Cu half-cells. CE of Li | Cu cells in a) carbonate electrolyte and b) ether electrolyte at  $0.5 \text{ mA cm}^{-2}$  with a cycling capacity of  $1.0 \text{ mAh cm}^{-2}$ . c) Charge and discharge curves of (a) at the 1st and 80th cycle. d) Corresponding electrochemical impedance spectra (EIS) of Li | Cu cells in (b) after the 1st cycle.

of Li | Li cells based on LiF-rich Cu is more stable than that of bare Cu (Figure S14).

Compared to the aforementioned strategies to suppress Li dendrites, the current concept of growing columnar Li through the LiF-rich Cu current collectors possesses following outstanding advantages: 1) the columnar Li deposition is dendrite-free, 2) the macroscopic structural color is a direct and effective descriptor to rapidly identify the microstructure of Li deposits, 3) the columnar Li film is versatile in various electrolytes including carbonate and ether, 4) the formation of aligned Li only depends on the LiF-rich initial layer and SEI but is independent on the type of conductive substrates; 5) the stripping/plating of Li columns after the first deposition is favored along the radial direction because of the thinner SEI on the side wall than on the tip and root, minimizing the volume effect of Li dissolution/deposition during cycling as the constant height of Li column showing (Figure S15);<sup>[16,18]</sup> 6) the method of controllable hydrolysis is facile and mild, benefiting easy handling and scaling-up; 7) the columnar Li is highly regulatable via interfacial chemistry design and pretreatment engineering; 8) ultrathin and microstructured Li anodes can be obtained with a specific capacity and exhibit great potential to match with Li-containing intercalated cathodes. Exemplified using a commercial lithium iron phosphate cathode, the stability of the full cell using the column Li metal anode is significantly enhanced (Figure S16). If a very stable and flexible SEI can be created on the columnar Li metal, such a thin Li metal anode is expected with dendrite-free morphology and very long lifespan in high-energy-density rechargeable batteries. This concept is quite versatile regardless the electrolytes and current collectors so that there are fruitful opportunities for it to be exerted in various Li metal batteries and to be improved through further engineering and coupling with advanced electrolytes and nanostructured current collectors.

In conclusion, a columnar Li metal anode was obtained on the LiF-rich Cu current collector. The LiF-rich SEI guided the deposited Li into an ordered and aligned columnar structure. Such an ultrathin Li anode exhibited significant improvement in performance such as stable cycling with high CE and long lives in both carbonate and ether electrolytes. This work provides not only a fresh viewpoint to investigate the deposition of Li through the complex energy chemistry at the interfaces of current collector/Li metal/electrolyte, but also an emerging ordered, dendrite-free, ultrathin Li metal anode for safe Li metal batteries.

### Acknowledgements

This work was supported by National Key Research and Development Program (grant numbers 2016YFA0202500 and 2015CB932500), Natural Scientific Foundation of China (grant number 21676160), and Tsinghua National Laboratory for Information Science and Technology. We thank Chong Yan, Chen-Zi Zhao, Xiao-Ru Chen, Ge Zhang, and Xin Shen for helpful discussion.

### Conflict of interest

The authors declare no conflict of interest.

**Keywords:** dendrites · electrochemistry · lithium deposition · lithium fluoride · nucleation

**How to cite:** *Angew. Chem. Int. Ed.* **2017**, *56*, 14207–14211  
*Angew. Chem.* **2017**, *129*, 14395–14399

- [1] M. Armand, J. M. Tarascon, *Nature* **2008**, *451*, 652; S. Chu, Y. Cui, N. Liu, *Nat. Mater.* **2016**, *16*, 16; H.-J. Peng, J.-Q. Huang, X.-B. Cheng, Q. Zhang, *Adv. Energy Mater.* **2017**, *7*, 1700260; H.-J. Peng, J.-Q. Huang, Q. Zhang, *Chem. Soc. Rev.* **2017**, *46*, 5237.
- [2] J. M. Tarascon, M. Armand, *Nature* **2001**, *414*, 359; J. B. Goodenough, K. S. Park, *J. Am. Chem. Soc.* **2013**, *135*, 1167; Y. Guo, H. Li, T. Zhai, *Adv. Mater.* **2017**, *29*, 1700007; X.-B. Cheng, R. Zhang, C.-Z. Zhao, Q. Zhang, *Chem. Rev.* **2017**, *117*, 10403.
- [3] W. Xu, J. L. Wang, F. Ding, X. L. Chen, E. Nasybutin, Y. H. Zhang, J. G. Zhang, *Energy Environ. Sci.* **2014**, *7*, 513.
- [4] D. Lin, Y. Liu, Y. Cui, *Nat. Nanotechnol.* **2017**, *12*, 194; K. Zhang, G.-H. Lee, M. Park, W. Li, Y.-M. Kang, *Adv. Energy Mater.* **2016**, *6*, 1600811.
- [5] A. Pei, G. Zheng, F. Shi, Y. Li, Y. Cui, *Nano Lett.* **2017**, *17*, 1132.
- [6] D. Aurbach, *J. Power Sources* **2000**, *89*, 206; K. Xu, *Chem. Rev.* **2014**, *114*, 11503; X.-B. Cheng, C. Yan, X. Chen, C. Guan, J.-Q. Huang, H.-J. Peng, R. Zhang, S.-T. Yang, Q. Zhang, *Chem* **2017**, *2*, 258; J. Qian, W. A. Henderson, W. Xu, P. Bhattacharya, M. Engelhard, O. Borodin, J. G. Zhang, *Nat. Commun.* **2015**, *6*, 6362; N. W. Li, Y. X. Yin, J. Y. Li, C. H. Zhang, Y. G. Guo, *Adv. Sci.* **2017**, *4*, 1600400; F. Ding, W. Xu, G. L. Graff, J. Zhang, M. L. Sushko, X. Chen, Y. Shao, M. H. Engelhard, Z. Nie, J. Xiao, X. Liu, P. V. Sushko, J. Liu, J. G. Zhang, *J. Am. Chem. Soc.* **2013**, *135*, 4450; X. B. Cheng, R. Zhang, C. Z. Zhao, F. Wei, J. G. Zhang, Q. Zhang, *Adv. Sci.* **2016**, *3*, 1500213; C.-Z. Zhao, X.-B. Cheng, R. Zhang, H.-J. Peng, J.-Q. Huang, R. Ran, Z.-H. Huang, F. Wei, Q. Zhang, *Energy Storage Mater.* **2016**, *3*, 77; Y. Liu, D. Lin, P. Y. Yuen, K. Liu, J. Xie, R. H. Dauskardt, Y. Cui, *Adv.*

- Mater.* **2017**, *29*, 1605531; E. Markevich, G. Salitra, F. Chesneau, M. Schmidt, D. Aurbach, *ACS Energy Lett.* **2017**, *2*, 1321.
- [7] R. Khurana, J. L. Schaefer, L. A. Archer, G. W. Coates, *J. Am. Chem. Soc.* **2014**, *136*, 7395; X. Han, Y. Gong, K. K. Fu, X. He, G. T. Hitz, J. Dai, A. Pearse, B. Liu, H. Wang, G. Rubloff, Y. Mo, V. Thangadurai, E. D. Wachsman, L. Hu, *Nat. Mater.* **2017**, *16*, 572; N. W. Li, Y. X. Yin, C. P. Yang, Y. G. Guo, *Adv. Mater.* **2016**, *28*, 1853; G. Zheng, S. W. Lee, Z. Liang, H. W. Lee, K. Yan, H. Yao, H. Wang, W. Li, S. Chu, Y. Cui, *Nat. Nanotechnol.* **2014**, *9*, 618; K. Liu, A. Pei, H. R. Lee, B. Kong, N. Liu, D. Lin, Y. Liu, C. Liu, P. C. Hsu, Z. Bao, Y. Cui, *J. Am. Chem. Soc.* **2017**, *139*, 4815; W. Zhou, S. Wang, Y. Li, S. Xin, A. Manthiram, J. B. Goodenough, *J. Am. Chem. Soc.* **2016**, *138*, 9385; W. Luo, Y. Gong, Y. Zhu, Y. Li, Y. Yao, Y. Zhang, K. Fu, G. Pastel, C.-F. Lin, Y. Mo, E. D. Wachsman, L. Hu, *Adv. Mater.* **2017**, *29*, 1606042.
- [8] W. Liu, D. Lin, A. Pei, Y. Cui, *J. Am. Chem. Soc.* **2016**, *138*, 15443; X. B. Cheng, T. Z. Hou, R. Zhang, H. J. Peng, C. Z. Zhao, J. Q. Huang, Q. Zhang, *Adv. Mater.* **2016**, *28*, 2888; Y. Lu, S. K. Das, S. S. Moganty, L. A. Archer, *Adv. Mater.* **2012**, *24*, 4430.
- [9] J. Heine, S. Krüger, C. Hartnig, U. Wietelmann, M. Winter, P. Bieker, *Adv. Energy Mater.* **2014**, *4*, 1300815; C. P. Yang, Y. X. Yin, S. F. Zhang, N. W. Li, Y. G. Guo, *Nat. Commun.* **2015**, *6*, 8058; Y. Liu, D. Lin, Z. Liang, J. Zhao, K. Yan, Y. Cui, *Nat. Commun.* **2016**, *7*, 10992; R. Zhang, X.-B. Cheng, C.-Z. Zhao, H.-J. Peng, J.-L. Shi, J.-Q. Huang, J. Wang, F. Wei, Q. Zhang, *Adv. Mater.* **2016**, *28*, 2155; L.-L. Lu, Y. Zhang, Z. Pan, H.-B. Yao, F. Zhou, S.-H. Yu, *Energy Storage Mater.* **2017**, *9*, 31; Y. Sun, G. Zheng, Z. W. Seh, N. Liu, S. Wang, J. Sun, H. R. Lee, Y. Cui, *Chem* **2016**, *1*, 287; Q. Yun, Y.-B. He, W. Lv, Y. Zhao, B. Li, F. Kang, Q.-H. Yang, *Adv. Mater.* **2016**, *28*, 6932; S. Jin, S. Xin, L. Wang, Z. Du, L. Cao, J. Chen, X. Kong, M. Gong, J. Lu, Y. Zhu, H. Ji, R. S. Ruoff, *Adv. Mater.* **2016**, *28*, 9094.
- [10] Y. Lu, Z. Tu, L. A. Archer, *Nat. Mater.* **2014**, *13*, 961; Q. C. Liu, J. J. Xu, S. Yuan, Z. W. Chang, D. Xu, Y. B. Yin, L. Li, H. X. Zhong, Y. S. Jiang, J. M. Yan, X. B. Zhang, *Adv. Mater.* **2015**, *27*, 5241; D. Lin, Y. Liu, W. Chen, G. Zhou, K. Liu, B. Dunn, Y. Cui, *Nano Lett.* **2017**, *17*, 3731; X. Q. Zhang, X. B. Cheng, X. Chen, C. Yan, Q. Zhang, *Adv. Funct. Mater.* **2017**, *27*, 1605989.
- [11] L. Terborg, S. Nowak, S. Passerini, M. Winter, U. Karst, P. R. Haddad, P. N. Nesterenko, *Anal. Chim. Acta* **2012**, *714*, 121.
- [12] R. Zhang, X. R. Chen, X. Chen, X. B. Cheng, X. Q. Zhang, C. Yan, Q. Zhang, *Angew. Chem. Int. Ed.* **2017**, *56*, 7764; *Angew. Chem.* **2017**, *129*, 7872.
- [13] X. Chen, H.-J. Peng, R. Zhang, T.-Z. Hou, J.-Q. Huang, B. Li, Q. Zhang, *ACS Energy Lett.* **2017**, *2*, 795.
- [14] M. D. Tikekar, S. Choudhury, Z. Y. Tu, L. A. Archer, *Nat. Energy* **2016**, *1*, 16114.
- [15] Z. Z. Gu, H. Uetsuka, K. Takahashi, R. Nakajima, H. Onishi, A. Fujishima, O. Sato, *Angew. Chem. Int. Ed.* **2003**, *42*, 894; *Angew. Chem.* **2003**, *115*, 922.
- [16] Y. Zhang, J. Qian, W. Xu, S. M. Russell, X. Chen, E. Nasybulin, P. Bhattacharya, M. H. Engelhard, D. Mei, R. Cao, F. Ding, A. V. Cresce, K. Xu, J. G. Zhang, *Nano Lett.* **2014**, *14*, 6889.
- [17] F. Ding, W. Xu, X. L. Chen, J. Zhang, M. H. Engelhard, Y. H. Zhang, B. R. Johnson, J. V. Crum, T. A. Blake, X. J. Liu, J. G. Zhang, *J. Electrochem. Soc.* **2013**, *160*, A1894.
- [18] J. F. Qian, W. Xu, P. Bhattacharya, M. Engelhard, W. A. Henderson, Y. H. Zhang, J. G. Zhang, *Nano Energy* **2015**, *15*, 135.

Manuscript received: July 12, 2017

Revised manuscript received: August 31, 2017

Accepted manuscript online: September 3, 2017

Version of record online: September 22, 2017